

A Parametric Investigation on the Cyclotron Maser Instability Driven by Ring-beam Electrons with Intrinsic Alfvén Waves

Zi-Jin Tong,¹ Chuan-Bing Wang,^{1,2, a)} Pei-Jin Zhang,¹ and Jin Liu^{1,3}

¹⁾ *CAS Key Laboratory of Geospace Environment, School of Earth and Space Sciences, University of Science and Technology of China, Hefei, Anhui 230026, China*

²⁾ *Collaborative Innovation Center of Astronautical Science and Technology, China*

³⁾ *School of Resource Environment and Earth Science, Yunnan University, Kunming, Yunan 650091, China*

(Dated: 13 September 2018)

The electron-cyclotron maser is a process that generates intense and coherent radio emission in plasma. In this paper, we present a comprehensive parametric investigation on the electron-cyclotron-maser instability driven by non-thermal ring-beam electrons with intrinsic Alfvén waves which pervade the solar atmosphere and interplanetary space. It is found that both forward propagating and backward propagating waves can be excited in the fast ordinary (O) and extraordinary (X) electromagnetic modes. The growth rates of X1 mode are almost always weakened by Alfvén waves. The average pitch-angle ϕ_0 of electrons is a key parameter for the effect of Alfvén waves on the growth rate of modes O1, O2 and X2. For a beam-dominated electron distribution ($\phi_0 \lesssim 30^\circ$), the growth rates of the maser instability for O1, O2 and X2 modes are enhanced with the increase of Alfvén wave energy density. In other conditions, the growth rates of O1, O2 and X2 modes weakened with increasing Alfvén wave intensity, except that the growth of O1 mode may also be enhanced by Alfvén waves for a ring distribution. The results may be important for us in analyzing the mechanism of radio bursts with various fine structures observed in space and astrophysical plasmas.

^{a)}Electronic mail: cbwang@ustc.edu.cn, corresponding author.

I. INTRODUCTION

Electron-cyclotron-maser (ECM) instability is an appealing mechanism for direct amplification of radio radiation by non-thermal (energetic) electrons, which has been widely applied for explanations of high-power radio emissions from magnetized planets as well as other astronomical objects¹, and for microwave generation in the laboratory². Twiss³ and Schneider⁴ first pointed out independently that this induced emission mechanism can amplify electromagnetic wave at radio frequency which is close to the electron-cyclotron frequency and its harmonics in a magnetic field. Hirshfield and Wachtel⁵ demonstrated the ECM emission by microwave generation in a gyrotron with relativistic electrons in the laboratory. Within the space and astrophysical context, the ECM instability did not receive intensive attentions until the late 1970s when the Earth's auroral kilometric radiation (AKR) was successfully explained by Wu and Lee⁶ in terms of the cyclotron-maser mechanism. They realized that including the weakly relativistic effect could dramatically increase the efficiency of the amplification of electromagnetic wave. Since then, the ECM instability has been extensively investigated in the 1980s, and has gained increasing attention in the last three decades with its applications to various radio emissions beyond the Earth, for example, the solar radio bursts^{7–13}, the radio emission from magnetized planets in our solar system^{14–16} and the time-varying emission from magnetized blazar jets¹⁷. One can refer to the review literatures^{1,18,19} for more details about the fundamentals of this instability and its applications in astrophysics.

There are two necessary conditions for the excitation of ECM instability. The first condition is that the local electron plasma frequency is less than the electron-cyclotron frequency for significant excitation of the fast ordinary and extraordinary electromagnetic waves. This indicates that the background plasma density may be depleted in the radio source region as demonstrated by *in situ* observation in the source region of AKR²⁰. There are only few works published on the physical process for this density depletion. It is considered that the plasma is diluted by a magnetic-field-aligned electric potential drop^{1,21,22} for the Earth's AKR. For a plasma with low plasma-beta value such as in the solar corona, the density may be depleted due to magnetic compression or Alfvén waves excited in a magnetic flux tube by beams of energetic particles through pressure balance across the boundary of the flux tube^{23,24}.

The second condition is that the electrons possess a velocity distribution with a perpendicular population inversion which provides the energy to amplify the electromagnetic wave via wave-particle resonant interaction. A number of velocity-distribution models have been proposed and studied for cyclotron maser that occurs in different physical environments, such as the loss-cone distribution (or a ring distribution, the most famous one)^{6,25,26}, the ring-shell distribution^{27,28}, the horseshoe distribution (or partial-shell distribution)^{29,30} and the hollow ring-beam distribution^{31,32}. Basically, the electron velocity distribution for maser instability can be divided into two components, namely, a ring and a beam. The ring is the velocity component perpendicular to the ambient magnetic field, which is the energy source for the cyclotron-maser instability. The beam is the velocity component parallel to the ambient magnetic field line. The relative amplitude and distribution of these two components determine the pattern and position of the area where the distribution function has positive gradient $\partial F_e / \partial v_\perp$ in phase space, which further gives the wave modes that are unstable and correspondingly their growth rates, frequencies and wave propagation angles, because the resonance ellipse of an unstable wave mode should be located inside the region where $\partial F_e / \partial v_\perp > 0$. Here F_e and v_\perp are the electron velocity distribution function and the perpendicular velocity with respect to the ambient magnetic field.

It is well-known that large-amplitude intrinsic Alfvén waves are observed in the solar atmosphere and interplanetary space^{33–36}. Much work has been published discussing the roles of Alfvén waves in the heating and acceleration of solar corona and solar wind through resonant or non-resonant wave-particle interaction^{37–40}. Recently, it is found that the pre-existing Alfvén waves enhance the ECM instability⁴¹ driven by non-thermal electrons with a beam-feature distribution. The waves qualitatively affect the velocity distribution of energetic electrons via pitch-angle scattering. A beam distribution function can deform quickly to become a crescent-shaped distribution so that the cyclotron-maser instability can be excited. At the same time the intrinsic Alfvén waves may modify the classical cyclotron resonance processes.

In this paper, we discuss the influences of intrinsic Alfvén waves on the growth rate of cyclotron-maser instability driven by non-thermal ring-beam electrons. Comparing with previously theoretical work, in most of which the growth rates were calculated for a few special parameter values, a comprehensive parametric investigation on the dependence of growth rates on several parameters is done in the present paper so that we can gain a more

complete view on the maser excitation at different physical conditions. The results can provide important clues for us to explore the various fine features of radio emission observed in nature.

The organization of the paper is as follows. In Section 2, the model of the scattered ring-beam electron distribution function is introduced and the general formulae for the growth rate is described. In Section 3, some sample growth rate calculations are presented to show the general characteristics of the maser instability. In Section 4, we display the results from the comprehensive parametric investigation on the maximum growth rate. Finally, we conclude in Section 5.

II. MODEL OF THE DISTRIBUTION FUNCTION AND FORMULAE OF THE GROWTH RATE

A. Distribution of ring-beam electrons scattered by Alfvén waves

The ring-beam distribution is not an infrequent feature for non-thermal (energetic) electrons accelerated in space and astrophysical plasmas. For instance, based on the physics of collisionless shock waves, the reflected electrons from quasi-perpendicular shock layer is characterized by ring-beam or loss-cone-beam distribution^{42,43}, which can be the energy source for radio emission from collisionless shock^{32,44,45}. Solar type III radio bursts are produced by fast electron beams along open magnetic field line^{12,46–48}, which may also have a ring component if they are initially injected to the open field with an angle with respect to ambient field line from the magnetic reconnection site.

When there are pre-existing Alfvén waves, these waves can pitch-angle scatter the electrons. During the pitch-angle scattering, the electron energy is conserved in a frame moving with the Alfvén waves. If the beam component is the dominant velocity for the non-thermal electron without Alfvén waves, the pitch-angle scattering will mainly accelerate the electrons in the transverse direction and will increase the ring component. On the other hand, if the ring component is the dominant component without Alfvén waves, the pitch-angle scattered electrons will mainly spread their pitch-angle distribution. As a result, a partial-shell (or crescent-shaped) distribution emerges, and a spherical shell (or ring-shell) distribution may develop, depending on the intensity of the Alfvén waves. Introducing the momentum per

unit mass of rest electron $\mathbf{u} = \mathbf{p}/m_{e0}$, we model the scattered ring-beam electron distribution simply as follows.

$$F_e(u, \mu) = A \exp \left[-\frac{(u - u_0)^2}{\alpha^2} - \frac{(\mu - \mu_0)^2}{\beta^2} \right], \quad (1)$$

where $\mu = \cos \phi = u_{\parallel}/u$, and ϕ is the pitch angle, u_{\parallel} is the momentum parallel to the ambient magnetic field. The quantities, u_0 and μ_0 represent the average electron momentum and the cosine of the average pitch-angle ϕ_0 , α and β designate the momentum dispersion and the spread width in pitch angle, respectively. The value of β is proportional to the normalized energy density of Alfvén waves. On the basis of a preceding analytical study⁴⁹ we assume that $\beta^2 \approx 2B_w^2/B_0^2$, where B_w and B_0 are the strength of the Alfvén wave magnetic field and the background magnetic field, respectively. The normalization constant A is given by

$$\frac{1}{A} = \frac{\pi^{3/2}}{\sqrt{2}} \beta \alpha^3 e^{-u_0^2/2\alpha^2} D_{-3} \left(-\frac{\sqrt{2}u_0}{\alpha} \right) \left[\operatorname{erf} \left(\frac{1 - \mu_0}{\beta} \right) + \operatorname{erf} \left(\frac{1 + \mu_0}{\beta} \right) \right]. \quad (2)$$

Here, $\operatorname{erf}(x)$ is the error function and $D_{-3}(z)$ is the parabolic cylinder function⁵⁰. Some contour plots of the electron distribution given by equation (1) with different parameters are shown in figure 1.

B. General expression of the growth rate

We assume that the thermal electrons are the dominant electron species in plasma, and a tenuous component of non-thermal electrons are the energy source to amplify the fast electromagnetic waves. According to the cold plasma theory, the dispersion relation for the extraordinary (X) and ordinary (O) modes is given by

$$N_{\sigma}^2 = \varepsilon_{\sigma},$$

$$\varepsilon_X = 1 - \frac{\omega_{pe}^2}{\omega(\omega + \tau\Omega_e)}, \quad \varepsilon_O = 1 - \frac{\tau\omega_{pe}^2}{\omega(\tau\omega - \Omega_e \cos^2 \theta)}, \quad (3)$$

where N_{σ} is the refractive index, the subscript σ represents the wave mode, $\sigma = O$ is the ordinary (O) mode, and $\sigma = X$ is the extraordinary (X) mode, ω_{pe} and Ω_e are the ambient plasma frequency and electron-cyclotron frequency, ω and θ denote the wave angular frequency and the wave phase angle defined with respect to the ambient magnetic field, respectively. The parameter τ is defined as

$$\tau = \left(s + \sqrt{\cos^2 \theta + s^2} \frac{\omega_{pe}^2 - \omega^2}{|\omega_{pe}^2 - \omega^2|} \right), \quad s = \frac{\omega\Omega_e \sin^2 \theta}{2|\omega_{pe}^2 - \omega^2|}. \quad (4)$$

The general expression of the temporal growth rate of ECM instability is given by^{9,51}

$$\begin{aligned}\Gamma_\sigma &= \frac{\pi n_b}{2 n_0} \frac{\omega_{pe}^2}{\omega} \frac{1}{(1 + T_\sigma^2) R_\sigma} \sum_{m=-\infty}^{\infty} \int d^3\mathbf{u} (1 - \mu^2) \delta \left(\gamma - \frac{m\Omega_e}{\omega} - \frac{N_\sigma u \mu}{c} \cos \theta \right) \\ &\times \left\{ \frac{\omega}{\Omega_e} \left[K_\sigma \sin \theta + T_\sigma \left(\cos \theta - \frac{N_\sigma u \mu}{c} \right) \right] \frac{J_m(b_\sigma)}{b_\sigma} + J'_m(b_\sigma) \right\}^2 \\ &\times \left[u \frac{\partial}{\partial u} + \left(\frac{N_\sigma u}{c} \cos \theta - \mu \right) \frac{\partial}{\partial \mu} \right] F_e(u, \mu),\end{aligned}\quad (5)$$

with

$$\begin{aligned}T_X &= -\frac{\cos \theta}{\tau}, & T_O &= \frac{\tau}{\cos \theta}, \\ R_X &= 1 - \frac{\tau \omega_{pe}^2 \Omega_e (1 + U)}{2\omega(\omega + \tau \Omega_e)^2}, & R_O &= 1 + \frac{\tau \omega_{pe}^2 \Omega_e (1 - U) \cos^2 \theta}{2\omega(\tau \omega - \Omega_e \cos^2 \theta)^2}, \\ K_X &= \frac{\omega_{pe}^2}{\omega^2 - \omega_{pe}^2} \frac{\Omega_e \sin \theta}{\omega + \tau \Omega_e}, & K_O &= \frac{\omega_{pe}^2}{\omega^2 - \omega_{pe}^2} \frac{\tau \Omega_e \sin \theta}{\tau \omega - \Omega_e \cos^2 \theta}, \\ U &= \frac{\tau^2 - \cos^2 \theta}{\tau^2 + \cos^2 \theta} \frac{\omega^2 + \omega_{pe}^2}{\omega^2 - \omega_{pe}^2}, & b_\sigma &= \frac{\omega}{\Omega_e} N_\sigma u (1 - \mu^2)^{1/2} \sin \theta,\end{aligned}\quad (6)$$

where $\gamma = (1 + u^2/c^2)^{1/2}$ is the relativistic factor and we have replaced all γ outside the delta function by unity in the weakly relativistic approximation, n_b and n_0 denote the number densities of non-thermal electrons and background electrons, $J_m(b_\sigma)$ and $J'_m(b_\sigma)$ are the Bessel function of order m and its first derivative, respectively. Here, we would like to point out that the electron-cyclotron maser works, in principle, only for relativistic distribution. The distribution function equation (1) is a simple Maxwellian distribution with pitch-angle anisotropy, which is reasonable for weak relativity. Otherwise, it is better to use the Jüttner distribution, which is the relativistically generalized classical Maxwell-Boltzmann distribution^{52,53}. This is beyond the scope of this paper.

III. GENERAL PROPERTIES OF ELECTRON-CYCLOTRON-MASER INSTABILITY

One can calculate the growth rate of emission in X mode or O mode for a given electron distribution and the plasma-to-electron cyclotron frequency ratio ω_{pe}/Ω_e on the basis of equations (1) and (5), which is a function of the wave frequency ω and the propagation phase angle θ . In the present discussion, we investigate the fundamental and second harmonic O mode and X mode waves which are designated by O1, X1, O2 and X2 for abbreviation. In

principle, the third or higher harmonics can also be excited with the increase of ω_{pe}/Ω_e , but their growth rates are much lower than the values of the fundamental and second harmonic wave modes⁵¹.

Figure 2 shows the normalized growth rate Γ/Ω_e of wave modes O1, X1, O2 and X2, plotted as a function of the normalized wave frequency ω/Ω_e and the phase angle θ , for several values of ω_{pe}/Ω_e . In obtaining these numerical results, the input parameters in the distribution function are taken to be $u_0 = 0.3c$, $\alpha = 0.1u_0$, $\beta = 0.5$ and $\mu_0 = 0.5$ ($\phi_0 = 60^\circ$), namely, the distribution function shown in the right-top panel in figure 1 is used. Note that the frequency ratios ω_{pe}/Ω_e are not same for the cases results shown in different panels in figure 2. For each wave mode from left to right, the first, second and third rows display the results for the case that ω_{pe} is much less than Ω_e , the case of ω_{pe}/Ω_e near which the wave is most unstable, and the case of ω_{pe}/Ω_e that is near its upper limit for instability, respectively. The upper limit of ω_{pe}/Ω_e for the excitation of each wave mode is determined by the necessary that its cutoff frequency is not much greater than the fundamental or harmonic electron-cyclotron frequency, which are approximately equal to 0.3, 1.0, 1.4 and 2.0 for modes X1, O1, X2 and O2, respectively.

One can see from figure 2 that both forward propagating waves ($\theta < 90^\circ$) and backward propagating waves ($\theta > 90^\circ$) can be excited for all wave modes, and the growth rates of the former are larger than that of the later. When the ratios ω_{pe}/Ω_e are far away from their upper limit values for wave excitation, the most unstable waves propagate nearly perpendicular to the ambient magnetic field with phase angle $\theta \approx 90^\circ$ for O1, O2 and X2 mode, while the most unstable wave of X1 mode propagates more obliquely with $\theta \lesssim 80^\circ$. On the other hand, as ω_{pe}/Ω_e approaches its upper limit for instability, every mode becomes to be quasi-parallel propagation.

Figure 3 plots the maximum growth rate Γ_{max}/Ω_e (upper panel), the frequency ω_{max}/Ω_e (middle panel) at which the maximum growth occurs, and the wave propagation angle θ_{max} (bottom panel) corresponding to the maximum growths for each mode as a function of the frequency ratio ω_{pe}/Ω_e . The blue, red, black and green lines represent the results of X1, O1, X2 and O2 wave modes, respectively. As has been noted by many researchers, the maximum growth rates depend on the frequency ratio ω_{pe}/Ω_e for each mode which can be unstable in a finite range of ω_{pe}/Ω_e . With the increase of ω_{pe}/Ω_e , modes X1, O1, X2 and O2 are stabilized in subsequence, and the propagation angle for all modes changes from

quasi-perpendicular direction to quasi-parallel direction before the modes are suppressed. At the same time, the frequencies of each mode start very close to the harmonic cyclotron frequency $m\Omega_e$ ($m = 1, 2$) but systematically deviate away from the harmonic frequency as ω_{pe}/Ω_e approaching its upper limit for instability.

These cases studies give us a brief survey on several basic properties of the ECM instability, which are generally similar for different models of electron velocity distribution shown in figure 1.

IV. DEPENDENCE OF GROWTH RATE ON THE INTENSITY OF ALFVÉN WAVES

To investigate the influences of Alfvén waves on the maser instability, we have done a comprehensive parametric calculation on the variations of the maximum growth rate with the parameters α , β , u_0 and μ_0 in the distribution function equation (1) for a given ω_{pe}/Ω_e .

As one can see from figure 3, the maximum growth rates of each wave mode first increase with increasing ω_{pe}/Ω_e to a peak value, then sharply drop as ω_{pe}/Ω_e approaching its upper limit for instability. The growth rates peak at $\omega_{pe}/\Omega_e \approx 0.15$, 0.7 for X1 and O1 modes, and at $\omega_{pe}/\Omega_e \approx 1.1$ for both X2 and O2 modes. The variation tendencies of the maximum growth rate with ω_{pe}/Ω_e are generally similar for different electron velocity distributions. Thus, without loss of generality, we let ω_{pe}/Ω_e equal to 0.15, 0.7, 1.1 and 1.1 for X1, O1, X2 and O2 modes respectively in what follows.

Firstly, we discuss the influence of Alfvén waves on the growth rate of maser instability excited by ring-beam electrons with different average pitch-angles. Contour plots of the maximum growth rate as function of ϕ_0 and β are presented in figure 4, where $\phi_0 = \arccos \mu_0$ is the average pitch-angle, and $\beta^2 \approx 2B_w^2/B_0^2$ is proportional to the magnetic field intensity of Alfvén waves. In these calculations, we choose $u_0 = 0.3c$ and $\alpha = 0.1u_0$. The left-top, right-top, left-bottom and ring-bottom panels are results for O1, O2, X1 and X2 modes, respectively. The results indicate that the dependencies of the growth rate on the strength of Alfvén waves are not only different for different wave mode, but also are different for different average pitch-angle of the ring-beam electrons.

For the O1 mode, the growth rates increase with the increase of β for pitch-angle $\phi_0 \lesssim 30^\circ$ and $\phi_0 \gtrsim 70^\circ$, while the growth rates decrease with the increase of β for $30^\circ < \phi_0 < 70^\circ$.

These imply that whether the non-thermal electron distribution are predominant by the beam component or the electrons are nearly a pure ring, the pre-existing Alfvén waves will enhance the growth of the maser instability of O1 mode. If the amplitude of the ring and beam components are comparable with each other, the pre-existing Alfvén wave will weaken the growth of the maser instability. For a giving intensity of Alfvén waves, if the intensity is not very strong, for example $\beta < 0.5$, the growth rates of ring-beam electrons with comparable two components are generally larger than that of beam-dominated electrons or pure ring electrons with the same electron energy. However, the growth rate of beam-dominated electrons becomes the largest one if the Alfvén wave intensity is strong enough with $\beta \gtrsim 0.6$.

For the O2 mode, the growth rates increase with the increase of β for $\phi_0 < 25^\circ$. This indicates that Alfvén waves enhance the maser excitation of O2 mode by beam-dominated non-thermal electrons, which is similar to the O1 mode. Meanwhile, the Alfvén waves have a weakening effect on the maser instability for $\phi_0 > 30^\circ$. Another interesting point is that the effects of Alfvén wave intensity on the O2 mode approach quickly to a saturated level at $\beta \approx 0.3$.

For the X1 mode, the growth rates decrease almost always with the increase of β , except in a very small region near $\phi_0 = 90^\circ$ where the growth rates first increase slightly, then decrease with the increase of β . This means that the pre-existing Alfvén waves have a weakening effect on the growth of X1 mode in general.

For the X2 mode, the growth rates increase greatly with the increase of β for pitch-angle $\phi_0 \lesssim 50^\circ$, while the growth rates decrease slowly with the increase of β for other pitch-angles. These indicate that Alfvén waves enhance the maser excitation of X2 mode driven by beam-dominated electrons, but weaken the maser instability produced by ring-dominated electrons.

In brief summary, if the velocity distribution of non-thermal electrons for maser instability are dominated by a beam component, the pre-existing Alfvén waves will enhance the growth rate of instability for O1, O2 and X2 modes but weaken the growth rate of X1 mode. For non-thermal electrons with a ring distribution, Alfvén waves can also enhance the growth rate of the fundamental mode, but weaken the growth rate of the second harmonic mode. If the non-thermal electrons have a velocity distribution with comparable beam and ring components, Alfvén waves generally weaken the growth rate of all wave modes.

Next, figure 5 shows the contour plots of the maximum growth rate as function of the average pitch-angle ϕ_0 and the average electron momentum u_0 . The other parameters used for these calculations are $\alpha = 0.03c$ and $\beta = 0.5$. The left-top, right-top, left-bottom and right-bottom panels are results for O1, O2, X1 and X2 modes, respectively. In general, the growth rates of all wave mode have an increasing trend with respect to the increase of electron momentum. For a fixed value of the average electron momentum (or energy), figure 5 seems to indicate that the growth rates of ring-dominated electrons are larger than that of beam-dominated electrons for X2 mode, while it is reversed for other wave modes. However, these are correct only for $\beta \gtrsim 0.5$ when the spread of the electron pitch-angle is scattered wide enough by intense Alfvén waves. Otherwise, as one can see from figure 4, for the pitch-angle spread width $\beta \lesssim 0.4$, the maximum growth rates peak at the region where the pitch-angle ϕ_0 is about 40° to 60° for O1, O2 and X1 modes.

Finally, we have a discussion on the effect of electron momentum dispersion α which can also be considered as the “temperature” of the ring-beam electrons. The lower the value of α is, the “colder” the ring-beam is. On the basis of equation (1), one can expect intuitively that the colder the ring-beam is, the higher the growth rate would be, since the gradient of distribution function in the momentum space increases with the decrease of α . Indeed, this is consistent with the numerical results, which we don’t show. An interesting result found from the numerical calculation is that the wave growth rates are more sensitive to the variation of Alfvén wave intensity for “hotter” ring-beam electrons than that for “colder” ring-beam electrons. For example, when the parameter value β decreases from 1.0 to 0.1 with fixed parameter values $u_0 = 0.3c$, $\phi_0 = 60^\circ$ and $\omega_{pe}/\Omega_e = 1.1$, the maximum growth rates of O2 mode increase 3.06 times and 23.2 times for $\alpha = 0.01c$ and $\alpha = 0.09c$ (corresponding to a “temperature” about 3.0×10^5 k and 2.4×10^7 k), respectively.

V. CONCLUSION

Large amplitude Alfvén waves intrinsically pervade the solar atmosphere and interplanetary space. Their roles on the heating and acceleration of solar corona and solar wind have been the hot and frontier research field for more than half centuries. Recently, it is suggested that Alfvén waves play important roles on the ECM instability^{23,24,41}. The electron-cyclotron maser is a process that can generate coherent radio radiation directly from non-thermal elec-

trons in magnetized plasma, which has been one of the dominant mechanism for producing high-power radio emissions observed in our universe¹. In this paper, we present a comprehensive parametric investigation on the influences of Alfvén waves on the cyclotron-maser instability driven by non-thermal ring-beam electrons.

It is found that both forward propagating and backward propagating waves can be excited in the X mode and O mode near the fundamental and harmonic electron-cyclotron frequencies in a finite range of frequency ratio ω_{pe}/Ω_e . The X1 mode propagates more obliquely with respect to the ambient magnetic field while O1, O2 and X2 modes propagate quasi-perpendicularly in general. However, each mode becomes to be quasi-parallel propagation as the frequency ratio ω_{pe}/Ω_e approaches its upper limit for instability.

Whether the pre-existing Alfvén waves enhancing or weakening the instability depend not only on the wave mode but also on the relative amplitude of the ring and beam components in the electron velocity distribution. The growth rates of X1 mode are weakened by Alfvén waves in general. For a beam-dominated distribution (the electron average pitch-angle $\phi_0 \lesssim 30^\circ$), the growth rates of maser instability for O1, O2 and X2 mode are enhanced with the increase of Alfvén wave energy density. In the other conditions, the growth rate of O1, O2 and X2 mode weaken with the increasing Alfvén wave intensity, except that the growth rate of O1 mode may also be enhanced by Alfvén waves for a ring distribution. In addition, the growth rates are more sensitive to the variation of Alfvén wave intensity for “hotter” ring-beam electrons than that for “colder” ring-beam electrons.

An implicit assumption in this study is that the electron distribution function does not change with time. In real situation, the electron velocity distribution may evolve with time. For instance, when the non-thermal electrons travel along the magnetic field line with decreasing background magnetic field strength, their average pitch-angle will decrease due to the conservation of magnetic moment, so that the electrons may evolve from a ring-predominant distribution to a beam-dominated distribution, or vice versa; the non-thermal electrons may lose some of their energy via collisions with the ambient plasma; and the energy density of Alfvén waves experienced by the evolving electrons may also vary with position and time. All of these can affect the spectral intensity, polarization, directivity and other properties of the radio emission amplified by non-thermal electrons through the cyclotron-maser instability, so the above results is important for us to understand the mechanism for the radio bursts with various fine structures observed in space and astrophysical plasmas.

ACKNOWLEDGMENTS

The research is supported by the National Nature Science Foundation of China (41574167, 41421063) and the Fundamental Research Funds for the Central Universities (WK2080000077).

REFERENCES

- ¹R. A. Treumann, *Astron. Astrophys. Rev.* **13**, 229 (2006).
- ²K. R. Chu, *Rev. Mod. Phys.* **76**, 489 (2004).
- ³R. Q. Twiss, *Austr. J. Phys.* **11**, 564 (1958).
- ⁴J. Schneider, *Phys. Rev. Lett.* **2**, 504 (1959).
- ⁵J. L. Hirshfield, and J. M. Wachtel, *Phys. Rev. Lett.* **12**, 533 (1964).
- ⁶C. S. Wu and L. C. Lee, *Astrophys. J.* **230**, 621 (1979).
- ⁷D. B. Melrose and G. A. Dulk, *Astrophys. J.* **259**, 844, (1982).
- ⁸L. Vlahos, *Solar Phys.* **111**, 155, (1987).
- ⁹C. S. Wu, C. B. Wang, P. H. Yoon, H. N. Zheng and S. Wang, *Astrophys. J.* **575**, 1094, (2002).
- ¹⁰C. S. Wu, C. B. Wang, G. C. Zhou, S. Wang and P. H. Yoon, *Astrophys. J.* **621**, 1129, (2005).
- ¹¹G. Q. Zhao, L. Chen, Y. H. Yan, D. J. Wu, *Astrophys. J.* **770**, 75, (2013).
- ¹²C. B. Wang, *Astrophys. J.* **806**, 34, (2015).
- ¹³D. B. Melrose, and M. S. Wheatland, *Sol. Phys.* **291**, 3637, (2016).
- ¹⁴P. Zarka, *J. Geophys. Res.* **103**, 20159, (1998).
- ¹⁵D. A. Gurnett, W. S. Kurth, D. L. Kirchner, G. B. Hospodarsky, T. F. Averkamp, P. Zarka, A. Lecacheux, R. Manning, A. Roux, P. Canu, N. Cornilleau-Wehrlin, P. Galopeau, A. Meyer, R. Boström, G. Gustafsson, J.-E. Wahlund, L. Hlen, H. O. Rucker, H. P. Ladreiter, W. Macher, L. J. C. Woolliscroft, H. Alleyne, M. L. Kaiser, M. D. Desch, W. M. Farrell, C. C. Harvey, P. Louarn, P. J. Kellogg, K. Goetz, A. Pedersen, *Space Sci. Rev.* **114**, 395, (2004).
- ¹⁶J. D. Menietti, P. H. Yoon, S. Ye, B. Cecconi, and A. M. Rymer, *Ann. Geophys.* **28**, 1013, (2010).
- ¹⁷M. C. Begelman, R. E. Ergun, and M. J. Rees, *Astrophys. J.* **625**, 51, (2005).

- ¹⁸C. S. Wu, Space Sci. Rev. **41**, 215, (1985).
- ¹⁹R. Bingham, D. C. Speirs, B. J. Kellett, I. Vorgul, S. L. McConville, R. A. Cairns, A. W. Cross, A. D. R. Phelps, K. Ronald, Space Sci. Rev. **178**, 695, (2013).
- ²⁰R. F. Benson, W. Calvert, and D. M. Klumpar, Geophys. Res. Lett. **7**, 959, (1980).
- ²¹L. R. Lyons, J. Geophys. Res. **85**, 17, (1980).
- ²²J. Vedin, and K. Rönmark, J. Geophys. Res. **110**, 8207 (2005).
- ²³C. S. Wu, C. B. Wang, and Q. M. Lu, Sol. Phys. **235**, 317 (2006).
- ²⁴D. J. Wu, L. Chen, G. Q. Zhao, and J. F. Tang, Astron. Astrophys. **566**, 138 (2014).
- ²⁵R. A. Dory, G. E. Guest, and E. G. Harris, Phys. Rev. Lett. **14**, 131, (1965).
- ²⁶L. C. Lee, and C. S. Wu, Phys. Fluids **23**, 1348, (1980).
- ²⁷G. Bekefi, J. L. Hirshfield, and S. C. Brown, Phys. Rev. Lett. **122**, 1037, (1961).
- ²⁸D. J. Wu, and J. F. Tang, Astrophys. J. **677**, 125, (2008).
- ²⁹R. M. Winglee, and G. A. Dulk, Astrophys. J. **307**, 808, (1986).
- ³⁰I. Vorgul, B. J. Kellett, R. A. Cairns, R. Bingham, K. Ronald, D. C. Speirs, S. L. McConville, K. M. Gillespie, and D. R. Phelps, Phys. Plasmas **18**, 6501, (2011).
- ³¹K. R. Chu, and J. L. Hirshfield, Phys. Fluids **21**, 461, (1978).
- ³²P. H. Yoon, C. B. Wang, and C. S. Wu, Phys. Plasmas **14**, 2901, (2007).
- ³³J. W. Belcher, and L. Davis, J. Geophys. Res. **76**, 3534, (1971).
- ³⁴B. De Pontieu, S. W. McIntosh, M. Carlsson, V. H. Hansteen, T. D. Tarbell, C. J. Schrijver, A. M. Title, R. A. Shine, S. Tsunata, Y. Katsukawa, K. Ichimoto, Y. Suematsu, T. Shimizu, and S. Nagata, Science **318**, 1574, (2007).
- ³⁵S. W. McIntosh, B. De Pontieu, M. Carlsson, V. Hansteen, P. Boerner, and M. Goossens, Nature **475**, 477, (2011).
- ³⁶H. Li, C. Wang, John D. Belcher, J. He, and John D. Richardson, Astrophys. J. Lett. **824**, L2, (2016).
- ³⁷E. Marsch, C. K. Goertz, and K. Richter, J. Geophys. Res. **87**, 5030, (1982)
- ³⁸J. V. Hollweg, and P. A. Isenberg, J. Geophys. Res. **107**, 1147, (2002).
- ³⁹P. A. Isenberg, and B. J. Vasquez, Astrophys. J. **731**, 88 (2011).
- ⁴⁰C. B. Wang, B. Wang, and L. C. Lee, Sol. Phys. **289**, 3895, (2014).
- ⁴¹C. S. Wu, C. B. Wang, D. J. Wu, and K. H. Lee, Phys. Plasmas **19**, 2902, (2012).
- ⁴²C. S. Wu, J. Geophys. Res. **89**, 8857, (1984).
- ⁴³W. M. Farrell, J. Geophys. Res. **106**, 15701, (2001).

- ⁴⁴R. Bingham, B. J. Kellett, R. A. Cairns, J. Tonge, and J. T. Mendonca, *Astrophys. J.* **595**, 279, (2003).
- ⁴⁵G. Q. Zhao, L. Chen, and D. J. Wu, *Astrophys. J.* **786**, 47, (2014).
- ⁴⁶J. P. Wild, J. A. Roberts, and J. D. Murray, *Nature* **173**, 532, (1954).
- ⁴⁷P. A. Robinson, and I. H. Cairns, *Sol. Phys.* **181**, 363, (1998).
- ⁴⁸H. A. S. Reid, and H. Ratcliffe, *Res. Astron. Astrophys.* **14**, 773, (2014).
- ⁴⁹P. H. Yoon, C. B. Wang, and C. S. Wu, *Phys. Plasmas.* **16**, 2102, (2009).
- ⁵⁰I. S. Gradshteyn, and L. M. Ryzbik, in *Table of Integrals, Series, and Products* (Elsevier, Singapore, 2000).
- ⁵¹S.-Y. Lee, S. Yi, D. Lim, H.-E. Kim, J. Seough, and P. H. Yoon, *J. Geophys. Res.* **118**, 7036, (2013).
- ⁵²F. Jüttner, *Ann. Phys.*, **339**, 856, (1911).
- ⁵³R. A. Treumann, and W. Baumjohann, *Ann. Geophys.*, **34**, 737, (2016).

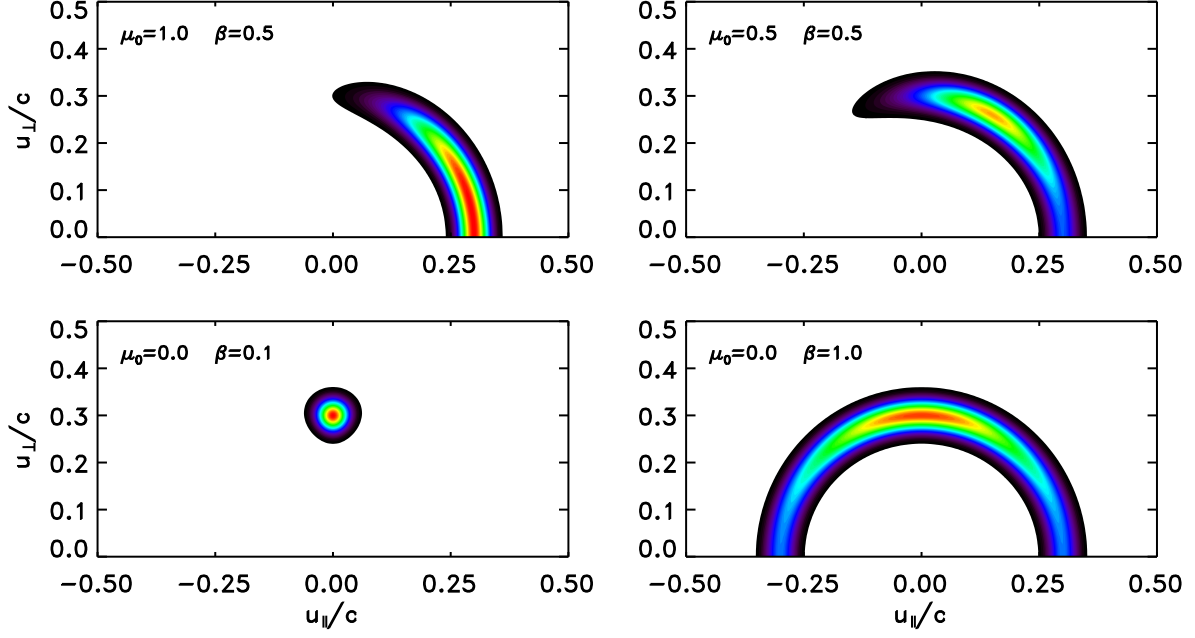


FIG. 1. Contour plots of the ring-beam non-thermal electron distribution function $F_e(u, \mu)$ versus u_{\perp} and u_{\parallel} in momentum space for different parameter values of μ_0 and β , where $u_0 = 0.3c$ and $\alpha = 0.1u_0$ are used for the plot in all panels.

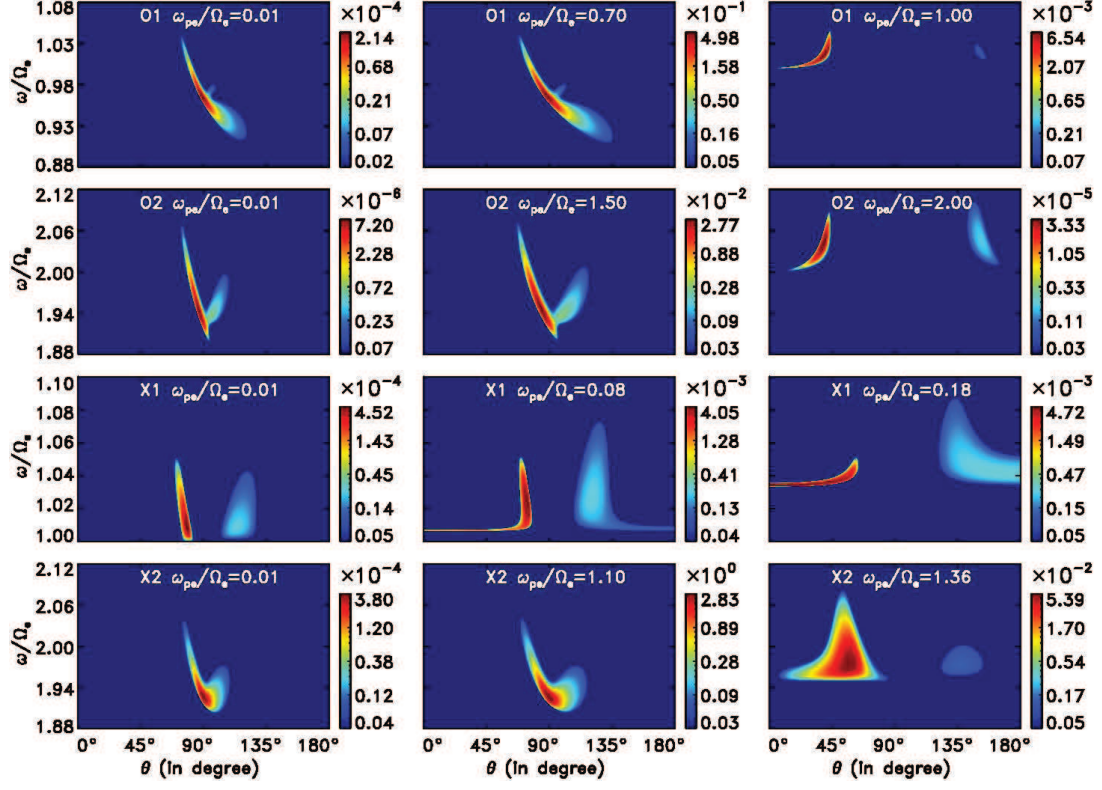


FIG. 2. Contour plots of the growth rate versus the wave propagation angle θ and wave frequency ω/Ω_e for the fundamental and harmonic X modes and O modes at different frequency ratio ω_{pe}/Ω_e for $u_0 = 0.3c$, $\alpha = 0.1u_0$, $\beta = 0.5$ and $\mu_0 = 0.5$.

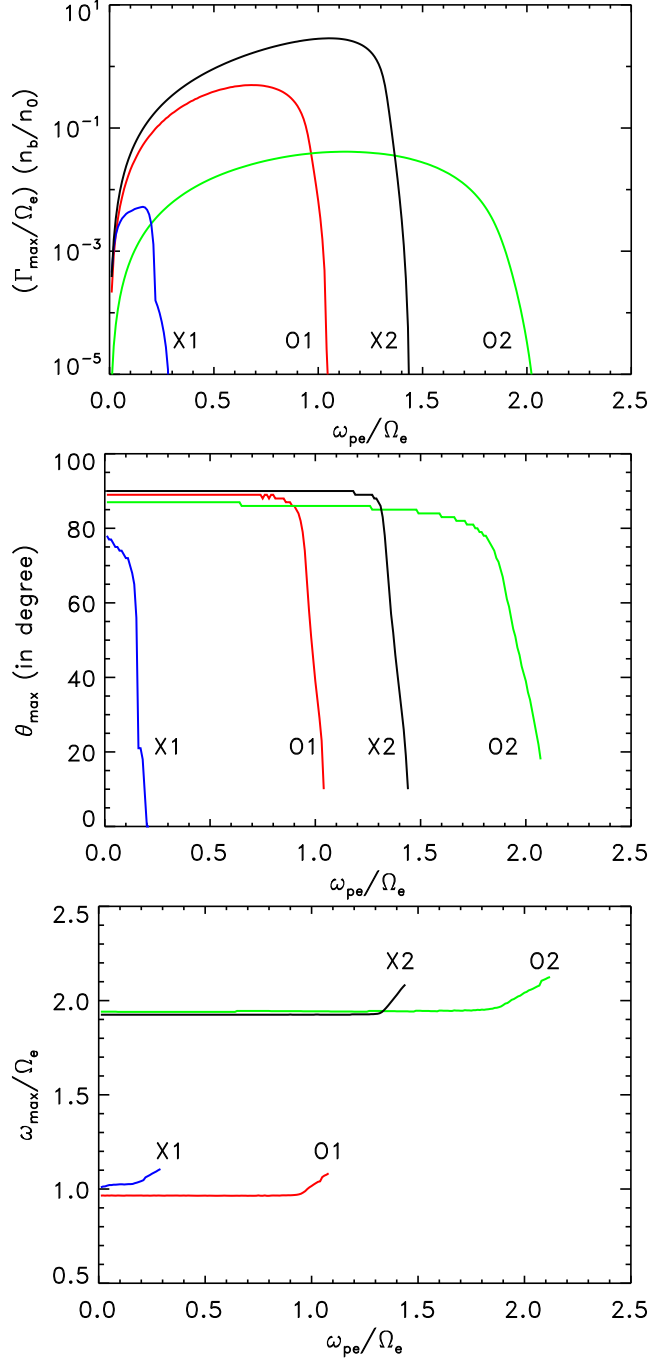


FIG. 3. The plot of the maximum growth rate Γ_{max}/Ω_e , propagation angle θ_{max} , and wave frequency ω_{max}/Ω_e as a function of the frequency ratio ω_{pe}/Ω_e for $u_0 = 0.3c$, $\alpha = 0.1u_0$, $\beta = 0.5$ and $\mu_0 = 0.5$.

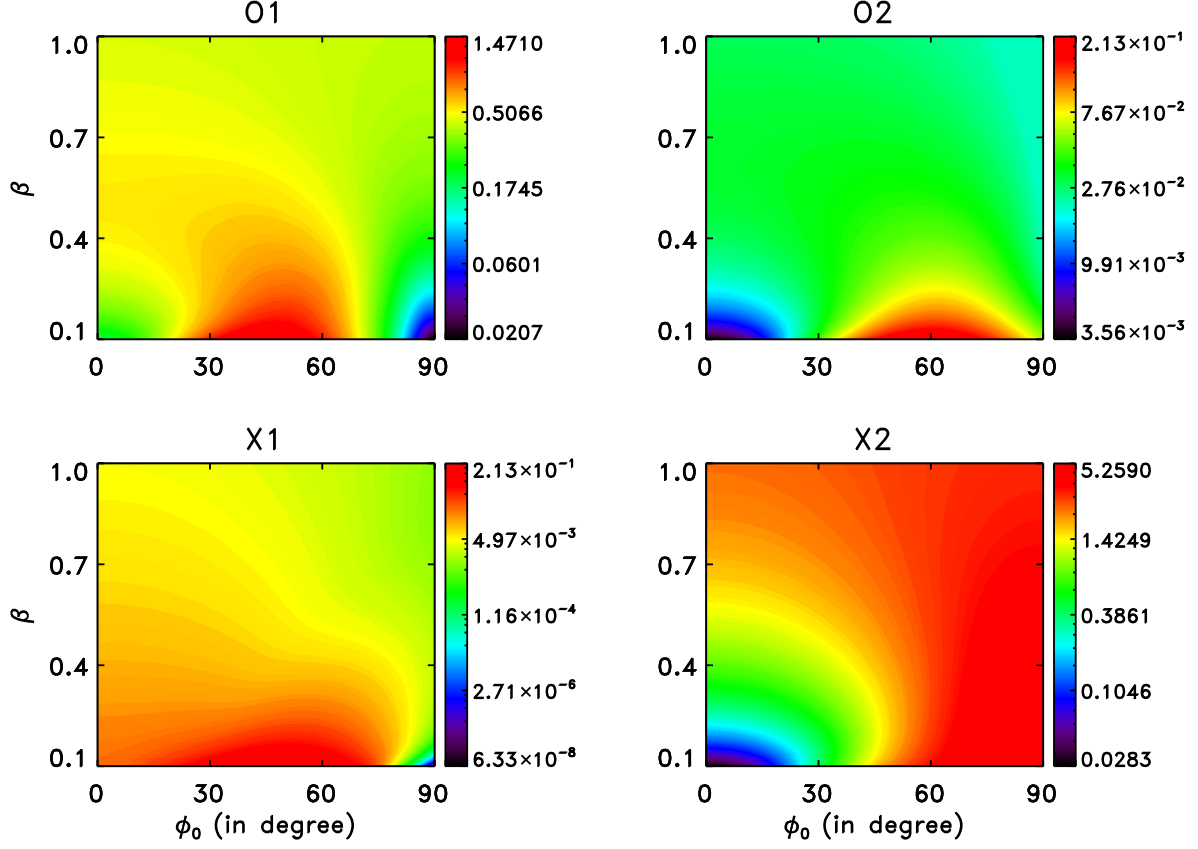


FIG. 4. Contour plots of the logarithm of the maximum growth rate versus electron average pitch-angle ϕ_0 and the spread width of pitch-angle β for $u_0 = 0.3c$ and $\alpha = 0.1u_0$. Note that β is proportional to the magnetic field intensity of Alfvén waves.

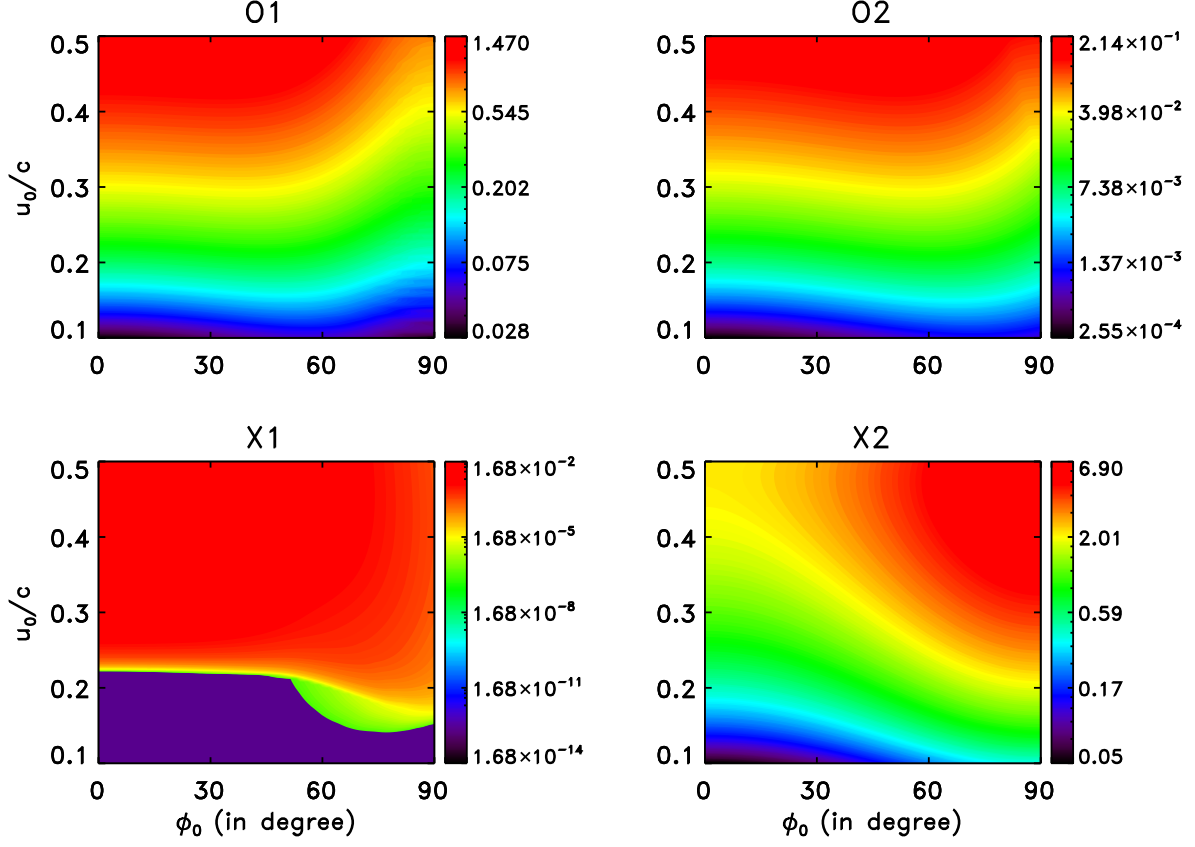


FIG. 5. Contour plots of the logarithm of the maximum growth rate versus average pitch-angle ϕ_0 and average electron momentum u_0 for $\alpha = 0.03c$ and $\beta = 0.5$.